Energy xxx (xxxx) 118072

Contents lists available at ScienceDirect

Energy

journal homepage: http://ees.elsevier.com

Comparative study of a bottoming SRC and ORC for Joule–Brayton cycle cooling modular HTR exergy losses, fluid-flow machinery main dimensions, and partial loads

Tomasz Kowalczyk [a,*], Janusz Badur [a], Paweł Ziółkowski [b]

[a] Energy Conversion Department, Institute of Fluid-Flow Machinery, Polish Academy of Sciences, Fiszera 14, 80-231, Gdańsk, Poland
[b] Gdańsk University of Technology, Department of Energy and Industrial Apparatus, Faculty of Mechanical Engineering, Narutowicza 11/12, 80-233, Gdańsk, Poland

ARTICLE INFO

Article history:
Received 3 December 2019
Received in revised form 3 June 2020
Accepted 4 June 2020
Available online xxx

Keywords
Partial load
Exergy
Heat transfer surface area
Last-stage blade length
Bottoming cycle

ABSTRACT

Energy conversion efficiency increase in power plants with high-temperature gas-cooled reactors via implementation of the bottoming cycle was investigated under nominal and minimal thermal load of a high-temperature reactor (HTR). Heat transfer surface area and turbine outlet volumetric flow rate in bottoming cycles was also investigated. Water and two low-boiling point working fluids (ammonia and ethanol) were analyzed. Analyzed thermodynamic cycles consisted of a closed Joule-Brayton cycle with helium as working medium, which was investigated in configurations with heat regeneration, compressor intercoolers, and in a simple design. Organic versus steam Rankine cycles were compared; low-boiling point fluids under supercritical conditions in some configurations provide higher cycle energy efficiency than the gas-steam cycle. Volumetric flow rates in the last turbine stages were reduced against the steam turbine to 38% and 0.8% with ethanol and ammonia, respectively. The steam Rankine cycle configuration provided the smallest heat transfer surface increase compared with the base cycle.

Nomenclature

A	free-cross section, m^2
B	exergy, kJ
$\dot{B}$	exergy rate, kW
b	specific exergy, kJ/kg or MeV/nucleon
D	diameter, m
E	energy, kJ or MeV/nucleon
g	weight fraction,
h	specific enthalpy, kJ/kg
k	overall heat transfer coefficient, kJ/(K*m^2)
$\dot{m}$	mass flow rate, kg/s
M	atomic mass
N	power, kW
N_A	Avogadro number, $6.022140857 \cdot 10^{26}$ n/kmol
p	pressure, bar
Q	heat, kJ
$\dot{Q}$	heat transfer rate or rate of heat flow, kW
s	specific entropy, kJ/(kgK)
S	surface of heat flow, m^2
T	temperature, K
$\dot{V}$	volumetric flow rate, m^3/s
v	velocity, m/s
W_F	nuclear fuel burnup level, MWd/kg
0101, …, 1601	points of the cycle
−01, …,-16	number of devices in the cycle

Greek symbols

δ	losses,
η	efficiency,
Δ	difference,
$\Delta\bar{T}$	logarithmic temperature difference, K
τ	coefficient of the free-flow area,
ξ	related losses,

Subscripts and superscripts

A	Inlet to a heat exchanger
B	Outlet from a heat exchanger
el	electric
ex	exergy
F	fuel
He	helium cooling the nuclear reactor
i	order number of fissionable element or isentropic process
m	mechanical

Acronyms

CHP	combined heat and power plant
CON	condenser

* Corresponding author.
E-mail addresses: tomasz.kowalczyk@imp.gda.pl (T. Kowalczyk); jb@imp.gda.pl (J. Badur); pawel.ziolkowski1@pg.edu.pl (P. Ziółkowski)

https://doi.org/10.1016/j.energy.2020.118072
0360-5442/

G	electric generator
GC	gas compressor
GCR	gas cooled reactors
GT	gas turbine
GTHTR300	gas turbine high temperature reactor of 300 MWe nominal rating
GT(R)	gas cycle with heat regeneration
GT(RI)	gas cycle with heat regeneration and intercooling
GT(R)-ORC	gas cycle with heat regeneration and with Organic Rankine Cycle as a bottoming cycle
GT(RI)-ORC	gas cycle with heat regeneration and intercooler and with Organic Rankine Cycle as a bottoming cycle
GT(S)	simple closed gas turbine cycle
GT-SRC	gas cycle with steam Rankine cycle as a bottoming cycle
HE	heat exchanger
HTC	heat transfer coefficient
HP	high pressure
HTR	high temperature nuclear reactor
IP	intermediate pressure
JAEA	Japan Atomic Energy Agency
LP	low pressure
M	motor
ORC	organic Rankine cycle
P	pump
PEM	proton-exchange membrane
pp	percentage point
R	heat regeneration
RI	heat regeneration and intercooler of compression
RES	renewable energy sources
RPM	rotation per minute
S–I	sulfur-iodine thermochemical cycle
SG	steam generator
SMR	small modular reactors
SR	steam reheater
SRC	steam Rankine cycle
ST	steam turbine
VG	vapor generator
VHTR	very high temperature reactors
VT	vapor turbine

1. Introduction

Changes in the world electrical power generation structure, arising from development of renewable energy sources (RES), have directed nuclear industrial interests toward small modular reactors (SMR). This technology shows great potential for providing zero emission and energy efficient support for RES via expansion of power plants, heat and power stations, and polygeneration systems, such as hydrogen production, powered by nuclear fission [1]. It is assumed that thermal output power of an SMR can reach 600 MW, which would allow for modular design and dynamic load changes to provide safe power system operation. The cost reductions of this technology as compared to conventional large-output nuclear power stations arise from prefabrication and passive safety, which make those units as simple as possible. In some solutions, the reactor is sealed with fuel and after the fuel burns, the whole reactor is replaced. For example, in the Japan 4S project, the 10 MW_t core lifetime was estimated as 30 years of operation without on-side refueling, and the lifetime of 135 MW_t unit was estimated as 10 years without on-side refueling [2]. After the Fukushima Daiichi nuclear disaster, political and social support for nuclear power has declined. However, the nuclear sector is still growing. The World Nuclear Association summarized 2018 in the World Nuclear Performance Report 2019 [3]: (1) the world nuclear electricity generation increased in 2017 and exceeded 2563 TWh; (2) the electric capacity of world's 449 operable reactors was 397 GWe; and (3) nine new reactors were brought online with more under construction. Currently, more than one-fifth of global nuclear generation is located in nuclear power plants with the highest number in North America followed by Central Europe and Asia. In Asia, nuclear generation increased in 2017, while in North America and West and Central Europe, it remained almost constant. In a long-term analysis, West and Central Europe is the only region that has noted a decrease in nuclear power generation. Moreover, the Canadian Nuclear Safety Commission reviews SMR designs and received the first application for an SMR license at Chalk River [3].

One type of SMR is a gas-cooled reactor. Development of high temperature gas-cooled reactors creates an opportunity to combined nuclear power with hydrogen technologies. Such a combination of energy generation and storage technologies is beneficial because of increased flexibility of electric power generation. As presented in recent works by the authors [4,5], in periods of low electrical power demand and large RES production, thermal units can effectively produce hydrogen. It should be emphasized that thermal units must provide power reserves, which means they must be in standby condition, in a so-called hot reserve, or be operated at a minimum load. Production of hydrogen increases energy efficiency of power reserves and makes it possible to use electrical energy from RES and nuclear fission. Use of hydrogen instead of hydrocarbons in the transport sector eliminates carbon dioxide and dust emissions. Compared to lithium-ion batteries, production of proton-exchange membrane (PEM) fuel cells do not require cobalt and rare earth metals [6].

With respect to heat processing, the most promising and mature technology is gas-cooled thermal-neutron reactors. Gas-cooled reactors (GCR) have operated in the United Kingdom since 1956 [7]. The newest facilities built in 1988 archived a gross efficiency above 40% and are the most efficient nuclear power plants worldwide [8]. Design of those power plants was based on a steam Rankine cycle (SRC) with a steam generator heated by carbon dioxide, which cools the reactor in a closed loop without the gas turbine. In author's previous work, a similar design was analyzed for a marine steam power plant under nominal and partial loads [9].

However, the vast majority of modern gas-cooled reactor projects employ a closed Joule–Brayton gas cycle for cooling the reactor core and generating electrical energy, which is in line with the exergy analysis theory [10]. In the field of improvement of gas cycles, an interesting approach was proposed by Ziółkowski et al. [11] in which reduction of regenerative exchanger size and increase of cycle thermal efficiency was realized by implementation of a modified Szewalski's idea. The idea was based on thermal regeneration in an open-loop Joule–Brayton cycle using gas extraction from the turbine. The idea could be applied for closed-loop gas-cooled reactors. Another approach is presented in work of Bartnik and al [12]. in which a hierarchical gas–gas system was proposed for improving the open Joule–Brayton cycle. The results indicate that energy efficiency of proposed gas–gas cycle is a few percentage points higher than for the gas cycle with conventional heat regeneration. On the other hand, through about two times lower investment costs, production of electricity can be even lower than in case of the more efficient gas–steam cycle. Both improvements could be considered in case of gas-cooled reactors.

Currently, the most advanced project in area of gas cooled reactors, the so-called high temperature reactors (HTR) or very high temperature reactors (VHTR) are being investigated in China, Japan, and United States [2,13]. The baseline thermodynamic cycle for the ongoing work is a gas cooled reactor with a closed Joule–Brayton cycle developed by the Japan Atomic Energy Agency (JAEA) and called a gas turbine HTR of 300 MWe nominal rating (GTHTR300) as described in the work of Kunitomi et al. [14]. The main features of the power plant are presented in Table 1. In the work of Sato et al. [15] the GTHTR300 cycle efficiency exceeded 50% as a result of an increase in both the reac-

Table 1
Main thermodynamic parameters of the GTHTR cycle based on the work of Kunitomi et al. [14] and Sato et al. [15].

Parameter	Unit	Kunitomi et al. [14]	Sato et al. [15]
Reactor outlet temperature	˚C	850	950
Compressor inlet temperature	˚C	28	28
Regenerative heat exchanger efficiency	%	95.0	96.0
Compressor polytropic efficiency	%	90.5	91.3
Turbine polytropic efficiency	%	92.8	93.8
Cycle electric net efficiency	%	45.6	50.4

tor outlet temperature and turbomachinery internal efficiency. The thermodynamic cycle parameters are presented in Table 1.

In both calculations, pressure drops in the heat exchangers were in range of 0.8%–2.4%, and heat loss in the heat exchangers and the reactor were omitted. The resulting efficiency is relatively high as for the gas cycle; however, the adopted machinery parameters refer more to state-of-the-art than currently exploited power plants.

In Joule-Brayton cycle pressure drops in the gas loop and internal efficiency of turbomachinery have more significant impact on cycle efficiency than in the case of Rankine cycle. Namely, in the above described case, an increase of 1 pp of pressure drop in the regenerative heat exchanger decreases the cycle efficiency by 1.4 pp. A decrease in turbine efficiency of 1 pp causes a reduction in the cycle efficiency by 0.6 pp, and for the compressor, 1 pp of efficiency decrease causes a drop in cycle efficiency by 0.5 pp. In contrast, the analysis of the proposed SRC indicates barely 0.001 pp reduction in the bottoming cycle energy efficiency, which is caused by a 1 pp increase in pressure drop in the steam reheater SR-05 (Fig. 7). The decrease of 1 pp in the HP (ST-09 in Fig. 7) and IP (ST-11) steam turbines internal efficiency causes 0.06 pp decrease in the cycle efficiency. The influence of the feeding water pumps internal efficiency on the overall energy efficiency is much lower than for compressors in Joule-Brayton cycle. A 1 pp reduction in the pumps internal efficiency decrease the cycle energy efficiency by 0.004 pp. The component that contributes most to the cycle efficiency is LP (ST-12) steam turbine. A 1 pp drop in its internal efficiency translates into a 0.34 pp drop in the cycle energy efficiency.

The influence of pressure losses are particularly important for working fluids with high heat capacity ratios, such as helium or other monoatomic gases [16]. A high heat capacity ratio means that temperature changes caused by pressure changes are high. In practice, it means that relatively low temperatures can be achieved at the turbine outlet; however, large temperature increases occur in the compressors. That is the reason why pressure losses are more energy consuming for gases with high heat capacity ratio than in the case of low heat capacity ratio gases or liquids.

In the work of Jaszczur et al. [17], a different approach toward increasing cycle efficiency was presented. Namely, a nuclear gas-cooled reactor was combined with a gas–steam cycle. Moreover, in order to increase radiation safety, the reactor is cooled with helium in a primary loop, while the gas cycle in second loop is filled with a 50/50 mixture of helium and nitrogen. Nitrogen provides a higher gas cycle efficiency. For an HTR outlet temperature equal to 900 ˚C, the electrical net efficiency was established as 45%, and for a temperature increase to 1000 ˚C, it can reach 55%. The main assumptions of the cycle include several parameters: (1) turbine and compressor isentropic efficiency equal to 90% and heat exchanger efficiency equal to 97%. Additionally, the gas–steam cycle works in parallel with a sulfur–iodine (S–I) thermochemical cycle for hydrogen production. In this paper, the assumption was made that the S–I cycle has a 48% overall efficiency. The results show that if 10% of the HTR thermal capacity is directed toward hydrogen production, the overall system efficiency decreases to 37%. However, an exergy analysis conducted by the authors indicates almost constant exergy efficiency for combined hydrogen and electrical generation for variable hydrogen production [18]. This situation is opposite to that in combined heat and power (CHP) plants in which the exergy of hot water for district heating is clearly lower than the exergy of electricity. This situation arises from the definition of chemical exergy in which the heat of combustion basically plays the major role [10].

This paper contains a thermodynamic analysis of coupling a GTHTR with a bottoming cycle. The aim of the project is to increase energy conversion efficiency. However, the modular design of the reactor tends to minimize the extent of the bottoming cycle. Two different approaches were investigated: (1) steam Rankine cycle (SRC) and (2) organic Rankine cycle (ORC). The ORC was tested with two low-boiling-point fluids: (1) ammonia and (2) ethanol. In authors' previous work [19–21], five more low-boiling point working fluids were tested for bottoming cycle: (1) isobutane, (2) pentane, (3) propane, (4) R236ea, and (5) R245fa. However, they did not meet the high thermodynamic cycle parameters achieved by ammonia and ethanol. It should be mentioned that the selected fluids are commonly used in the industrial sector and are relatively cheap. Both cycles were compared with respect to energy efficiency for nominal and minimal loads, total heat transfer surfaces, and the last-stage turbine blade length. Dimensions of the low-pressure turbine outlet are more problematic in cases of bottoming cycles than in conventional steam turbine plants because feed water heaters are not normally found. The lack of water heaters causes more massive steam flow through the low-pressure part for the corresponding live steam mass flow rate. The difference can reach as much as 35% of the mass flow rate. The exergy calculus was employed to estimate thermodynamic losses in each device during the cycles.

2. Energy cycle design

To calculate the main parameters of the thermodynamic cycle, the in-house COM-GAS numerical code was employed.[1] Additionally, the main results were confirmed using one of the commercial codes. The COM-GAS code uses the zero-dimension balance of mass, momentum, and energy [11]. The heat transfer surface was calculated with an assumption of an overall heat transfer coefficient (HTC), whereas turbine blade lengths were calculated with an assumption of vapor/steam velocity. Detailed data are presented in section 2.2.

In the paper three energy cycles are investigated:

Gas Turbine Cycle GT:
- in configuration with heat regeneration and intercooler: GT (RI)
- in configuration with heat regeneration: GT(R)
- in simple configuration: GT

Gas Turbine Cycle with Organic Rankine Cycle as the bottoming cycle:
- in configuration with heat regeneration and intercooler: GT (RI)-ORC
- in configuration with heat regeneration: GT(R)-ORC

Gas Turbine Cycle with Steam Rankine Cycle as a bottoming cycle: GT-SRC.

The GT (RI) cycle is a reference cycle for which optimization of heat recovery and intercoolers was conducted. The scheme of the cycle is presented in Fig. 1.

During the analysis, the influence of heat regeneration and the compressor's intercooler on the cycle's energy efficiency was investigated and optimized. The gas cycle with heat regeneration and intercooling was termed GT (RI), cycle with suppressed intercooling GT(R), and a simple cycle with suppressed both intercooling and regeneration was called GT. Thermodynamic interpretation of the GT (RI) on the temper-

[1] The COM-GAS code was developed in the Energy Conversion Department Institute of Fluid Flow Machinery PASci.

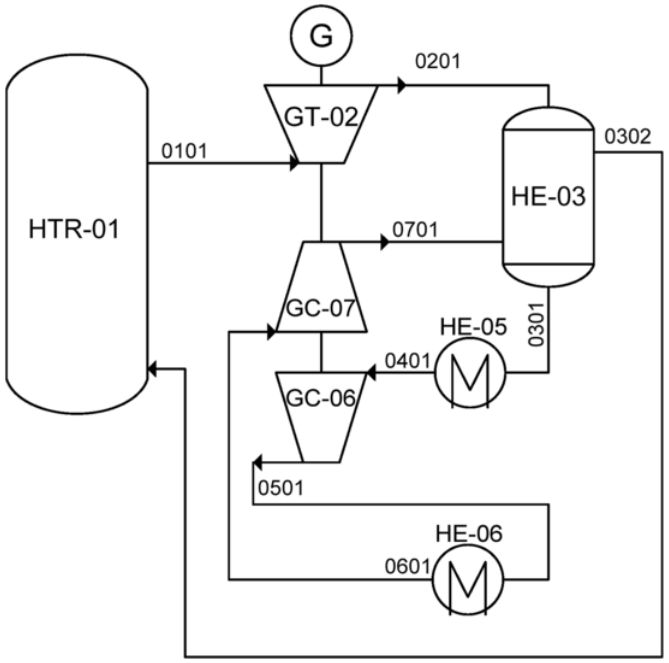

Fig. 1. Scheme of the Gas Turbine (GT cycle). HTR: high temperature nuclear reactor, GT: gas turbine, GC: gas compressor, HE: heat exchanger, and G: electrical generator.

ature-specific entropy diagram is presented in Fig. 2. Points of the cycle are consistent with the scheme in Fig. 1. Lines between points 0201 and 0301 and 0701 and 0302 represent the regenerative heat exchanger, named HE-03 in scheme in Fig. 1. It is assumed that helium is cooled to 35 °C in coolers HE-05 and -06. In the case of bottoming cycles condensers, the condensate temperature is assumed to be 33 °C because of higher heat transfer coefficients.

In this paper, the thermodynamic parameters of the machinery were based on currently operating units as done in work of Jaszczur et al. [17], which is opposite to the state-of-the-art approach presented in work of Kunitomi et al. [14]. The selected approach was dictated by caution resulting from lack of experience in design and maintenance of large power helium turbomachinery [22,23]. Moreover, in combined cycles, the gas cycle to the bottoming cycle efficiency ratio is essential during the optimization process. Thermodynamic parameters of cycle components for nominal conditions are presented in Table 2.

The heat source of each cycle is a 600 MW thermal capacity helium-cooled high-temperature reactor (HTR). For coal-fired boilers of thermal capacity around 600 MW, heat losses through convection and radi-

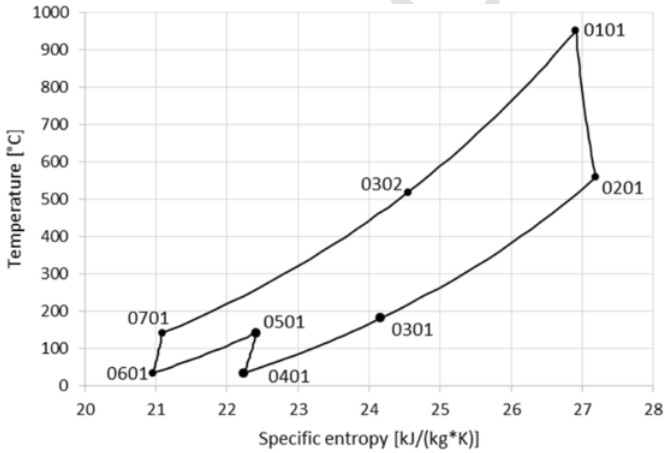

Fig. 2. Thermodynamic heat regeneration and intercooler (GT [RI]) effects on the temperature-specific entropy diagram. Cycle point are consistent with the scheme in Fig. 1.

Table 2
Main thermodynamic parameters of investigated cycles for nominal conditions.

Parameter	Symbol	Unit	Value
Reactor thermal power	$\dot{Q}_{HTR}$	MW	600
Helium temperature at the reactor outlet	$T_{HTR,max}$	°C	950
Stream of heat losses in the reactor	$\xi\dot{Q}_{HTR}$	–	0.00
Pressure drop of coolant in the reactor	ξp_{HTR}	–	0.05
Stream of heat losses in heat exchangers	$\xi\dot{Q}_{HE}$	–	0.02
Pressure drop of working fluid in heat exchangers and steam/vapor generators	ξp_{HE}	–	0.05
Isentropic efficiency of the gas turbine	$\eta_{i,GT}$	–	0.900
Isentropic efficiency of the ORC turbine	$\eta_{i,ORC}$	–	0.900
Isentropic efficiency of the steam/vapor turbine high pressure, intermediate pressure and low-pressure parts	$\eta_{i,ST\ HP}$	–	0.900
	$\eta_{i,ST\ IP}$		0.920
	$\eta_{i,ST\ LP}$		0.850
Isentropic efficiency of the gas compressor	$\eta_{i,GC}$	–	0.880
Isentropic efficiency of the pumps	η_P	–	0.850
Mechanical efficiencies of above machinery	η_m	–	0.998
Efficiencies of electric generators	$\eta_{el,G}$	–	0.992
Efficiencies of electric motors	$\eta_{el,M}$	–	0.950

ation on the walls are in range of 0.5%–1.0% of the nominal load. However, there are no data in the literature addressing those losses in cases of HTRs; therefore, the stream of heat losses in the reactor was omitted. The reactor outlet temperature was 950 °C. In the mathematical model, the reactor inlet temperature resulted from the cycles configuration and thermodynamic parameters of the machinery, primarily the gas cycle compression ratio and heat transfer surfaces area. However, the reactor inlet temperature strongly affects the reactor's exergy efficiency. Namely, for higher temperature the exergy destruction in the core is lower; therefore, the reactor inlet temperature was described in detail in the Results section.

Given isentropic efficiencies of the turbine parts refer to the nominal load. However, those values were almost constant for partial loads because isentropic efficiency is described in the flow section. Throttling in control valves was considered independently of the turbine. In case of the LP turbine under minimal load, the influence of centrifugal force acting on the steam jet directing it to the upper part of the blades, causing a vortex and backflow at the blade foot, was also omitted. The geometrical conditions of turbine stages were not considered, so a possibility of work in the ventilation conditions was also omitted. The efficiencies of the electric generators and motors were assumed to be constant.

In bottoming cycles, only so-called wet working fluids were analyzed. This type of fluids feature a negative slope on the saturated vapor curve. The dry fluids feature a positive slope, whereas the isentropic fluids feature practically a vertical saturation curve. This choice follows the results of the author's previous works [19–21,24] and the work of Mikielewicz et al. [25], where ammonia, ethanol, isobutane, pentane, propane, R236ea and R245fa were analyzed. For ORC turbine inlet temperature in the range of 45–120 °C, ethanol provides the highest energy efficient of the bottoming cycle. The cycles efficiency achieved with ammonia is only slightly lower, however ammonia provides the smallest volumetric flow rates. Both, ammonia and ethanol, provide the smallest mass flow rates in the bottoming cycles among the analyzed low-boiling point fluids.

Another remarkable result of the cited works is the lower efficiency in terms of the First Law of Thermodynamics of ORCs with dry fluids that operate without regenerative heat exchanger between the turbine and the condenser. In a large-scale bottoming cycle, the heat transfer surfaces should be limited, which means that bottoming turbine exhaust vapor should not be superheated. It should be emphasized that when considering thermodynamic cycles, the degree of dryness at the turbine outflow is > 0.92, so condensing liquid drops do not threaten machine safety. The saturation curves for the selected fluids are shown in Fig. 3.

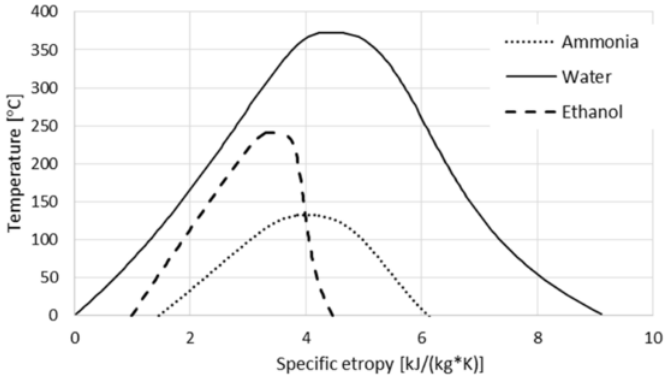

Fig. 3. Saturation curves of selected working fluids for bottoming cycle: (1) water; (2) ammonia; and (3) ethanol.

A specific working fluid for the Rankine cycle is ammonia. The saturation pressure for 33 °C is 12.70 bar, which caused small specific volume increases due to expansion in turbine. As a result, the increase in turbine blades height along the turbine was insignificant. Detailed results describing these findings are presented in Section 3. Differences between the thermodynamic parameters of both low-boiling point working fluids and the assumed HTR inlet temperature of approximately 450 °C made it necessary to carry out the optimization of heat regeneration, compressor intercooling, and compression ratio. The scheme of the combined cycle with the ORC bottoming cycle is presented in Fig. 4.

Thermodynamic interpretation of the GT(R)-ORC with ethanol as a working fluid is presented in Fig. 5, while the GT (RI)-ORC with ammonia is shown in Fig. 6. In both cases, diagrams present the optimal configuration of the cycles and working fluid selection with respect to energy efficiency. In both cases, the highest efficiency was reached for suppressed HE-05 and -08 helium coolers. As mentioned earlier, the condensate temperature is assumed to be 33 °C.

The main difference between ammonia and ethanol as the bottoming cycle working fluid was optimal ORC turbine inlet temperature, which was >200 K lower in the case of ammonia. This imposed a higher heat transfer rate in HE-03. On the diagram in Fig. 5, it is clearly visible that in the case of GT(R)-ORC, the temperature range of HE-03 operation was <50 K, while in case of GT (RI)-ORC it was >250 K.

The steam Rankine cycle, because of much higher enthalpy change during the phase change process, is equipped in steam reheater. The steam turbine was divided into three parts: (1) high pressure (ST-09); (2) intermediate (ST-11); and (3) low pressure (ST-12). Afterwards, steam from the high-pressure turbine outlet was mixed with the intermediate pressure steam from SG-07 steam generator and reheated in SR-05 steam reheater. Likewise, in the conventional combined gas-steam cycles there was no steam extraction and no thermal regeneration of the feed water. As it mentioned previously, using this approach caused an increase in the waste heat utilization but caused an increase in the size of the low-pressure turbine. To simplify the analysis, SRC without a deaerator was used. If there is a deaerator used, a feedwater preheater should be employed. On the one hand, if there is no deaerator, it is possible to lower the helium temperature at the compressor inlet. On the other hand, in contrast to the open loop combined cycles, in closed loop gas cycles higher temperature at the outlet of the steam generator is not a loss of heat. Moreover, the use of steam extraction reduces the heat flow rate lost in the condenser. There are known solutions to integrate the deaerator with the condenser [26,27]. The scheme of the combined cycle with the SRC bottoming cycle is presented in Fig. 7.

During the analysis, as mentioned earlier, the temperatures of working fluids at the CON-12/CON-13 condensers outlets were assumed to be 33 °C. The same condensation temperature was assumed for water and low-boiling point fluids despite higher HTC for the former, as the latter havelower volumetric flows in turn. In the GT-ORC, the helium preceding the inlet to the HE-05 and -08 heat exchangers was precooled in the VG-04 and -07 vapor generators. However, due to the optimization process for both ORCs, the HE-05 and -08 were suppressed, which increased the energy efficiency of heat utilization from the Joule–Brayton cycle. The compression ratios of GC-06 and -09 were adjusted to even out the temperatures of the working fluid at the VG-04 and -07 outlets. The optimization process indicates the lowest exergy destruction in the cycle for this configuration. In conventional open gas cycles with intercoolers, the compression ratios of the low and high pressure compressors are adjusted to even out the enthalpy increase in both machines [28]. The thermodynamic interpretation of the GT-SRC is presented in Fig. 8.

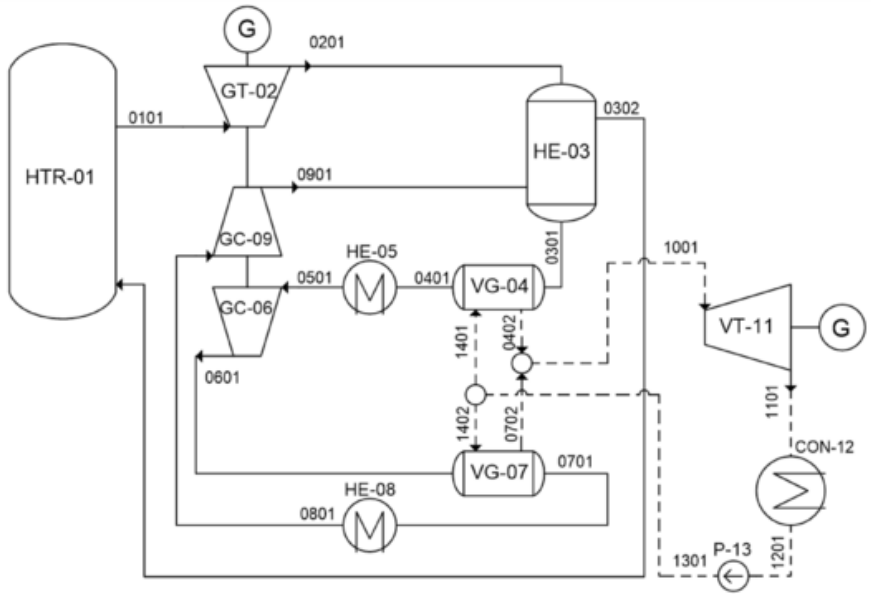

Fig. 4. Scheme of the Gas Turbine Cycle with Organic Rankine Cycle in configuration with heat regeneration and intercooler (GT [RI]-ORC). VG: vapor generator, VT: vapor turbine, P: pump, CON: condenser. Solid lines represent the gas cycle and dashed lines the ORC.

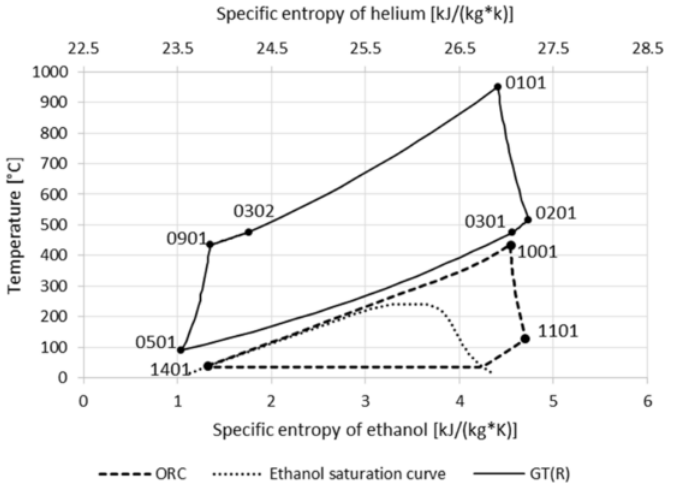

Fig. 5. Thermodynamic GT(R)-ORC effects on the temperature-specific entropy diagram. Cycle points are consistent with the scheme in Fig. 4.

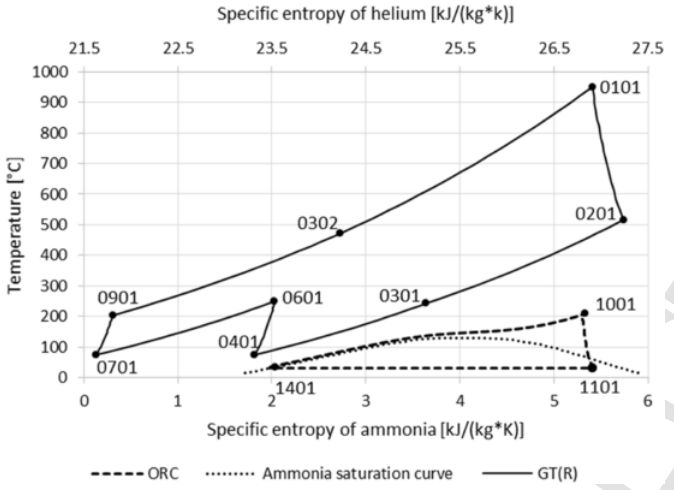

Fig. 6. Thermodynamic interpretation of the GT (RI)-ORC on the temperature-specific entropy diagram. Cycle points are consistent with the scheme in Fig. 4. Points 0701 and 0801 were equal because the HE-08 heat exchanger was suppressed.

The SG-04 steam generator works under large temperature differences and is shown in Fig. 8 between points 0201 and 0601 (helium cooling) and 1301 and 0402 (simplified visualization of high-pressure steam preheating, evaporation, and superheating. The SR-05 steam reheater cooling helium was almost in the same range of temperature; however, the increase in steam temperature was lower than in case of the SR-05. In Fig. 8, it is presented with lines 1001–0502. Diagrams of temperature in functions of exchange heat rate and calculations of exergy destruction are presented in later sections of this paper. Thermodynamic properties of working fluids in characteristic points of investigated cycles under nominal load is presented in Table A-1.

2.1. Power, exergy, and efficiency definitions

To conduct a comparative analysis, it is necessary to define basic parameters of the cycle output power, efficiency, and exergy losses. The cycle output power ($N_{el,net}$) is equal to sum of the sub-cycles electric net power as shown in the equation:

$$N_{el,net} = N_{el,GT} + N_{el,ORC/SRC} \tag{1}$$

In case of a gas cycle, the electric power $N_{el,GT}$ is a result of multiplication of electric generator efficiency and mechanical power on the turbo-generator shaft. The mechanical power on the shaft is equal to difference between the gas turbine and the compressor power. In the case of a steam or vapor cycle, the output power ($N_{el,ORC/SRC}$) is given as electric generator power minus the pump demand. According to the scheme in Fig. 4, the equations take the following forms:

$$N_{el,GT} = \eta_{el,G}\eta_m \left(N_{GT-02} - N_{GC-08}\right) \tag{2}$$

$$N_{el,SCR} = \eta_{el,G}\eta_m \left(N_{ST-9} + N_{ST-11} + N_{ST-12}\right) - \eta_{el,M}\eta_m \left(N_{P-14} + N_{P-16}\right) \tag{3}$$

in which $\eta_{el,G}; \eta_m; \eta_{el,M}$ are presented in Table 2. The exergy calculus was used to define streams of exergy losses in the main devices involved in the cycle. The stream of exergy losses is expressed in units of power and represents a loss of mechanical power during the cycle, which could be generated by the Carnot engine. For heat exchangers, the stream of exergy losses can be described as the difference between enthalpies of heating and heated medium, including changes in entropy. Using the example of a regenerative heat exchanger (HE-03) shown in Fig. 1, the equation can be written:

$$\begin{aligned}\delta\dot{B}_{HE-03} &= \dot{B}_{0201} - \dot{B}_{0301} - \left(\dot{B}_{0302} - \dot{B}_{0701}\right) \\ &= \dot{m}_{0201}\left(b_{0201} - b_{0301}\right) \\ &\quad - \dot{m}_{0701}\left(b_{0302} - b_{0701}\right) \\ &= \\ &= \dot{m}_{0201}\left[\left(h_{0201} - h_{0301}\right) - T_0\left(s_{0201} - s_{0301}\right)\right] \\ &\quad - \dot{m}_{0701}\left[\left(h_{0302} - h_{0701}\right)\right. \\ &\qquad \left. - T_0\left(s_{0302} - s_{0701}\right)\right]\end{aligned} \tag{4}$$

in which $\dot{B}$ is exergy rate, $\dot{m}$ is mass flow rate, T_0 means temperature of ambient, b, h, and s represent specific exergy, specific enthalpy,

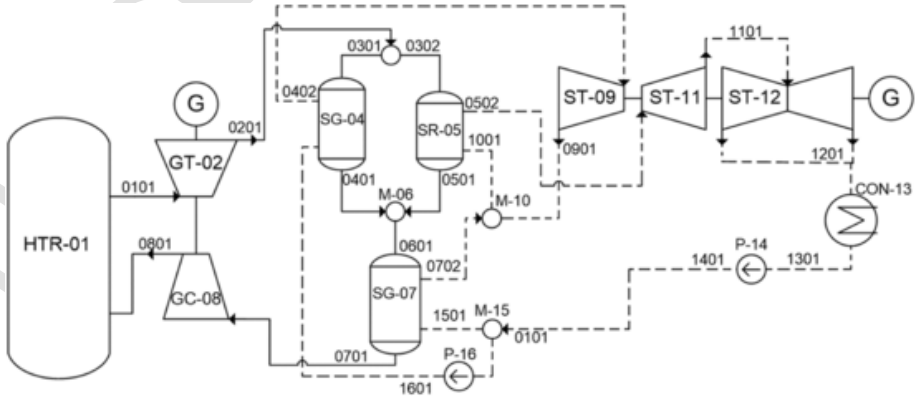

Fig. 7. Scheme of the Gas Turbine with steam Rankine cycle (GT-SRC). SG: steam generator, SR: steam reheater, ST: steam turbine. Solid lines represent the gas cycle, dashed lines the SRC.

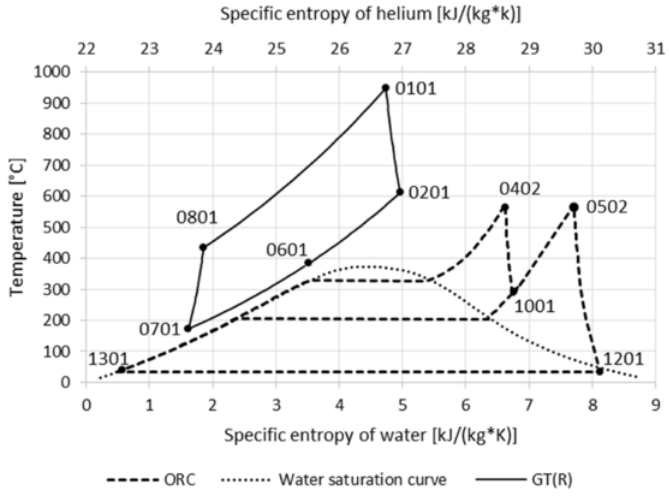

Fig. 8. Thermodynamic interpretation of the GT-SRC on the temperature-specific entropy diagram. Points of the cycle are consistent with the scheme in Fig. 7.

and specific entropy, respectively. Ambient conditions for exergy calculations are determined in accordance with ISO 3977 standards for gas turbine measurements, namely 15 ˚C and 101.3 kPa.

To calculate the exergy losses in the nuclear reactor, in addition to cooling gas parameters, knowledge of fuel parameters is necessary. Based on the experimental HTR-10 operational data [29], the following assumptions were imposed:

Uranium enrichment level 17%
Fission exergy of U_{235} $b_{fis,U235}$ = 192.9 MeV/nucleon
Fission energy of U_{235} $e_{fis,U235}$ = 202.5 MeV/nucleon
Fuel (heavy metals) burnup W_F = 80 MWd/kg

The stream of the exergy losses in the reactor can be expressed by the equation:

$$\delta \dot{B}_{HTR} = \dot{B}_F - \left(\dot{B}_{He,OUT} - \dot{B}_{He,IN}\right) \tag{5}$$

The exergy stream of fuel can be determined by the equation:

$$\dot{B}_F = \mathrm{N}_A \sum_{i=1}^{j} \left(\frac{1.60217662 \cdot 10^{-16} b_{\mathrm{fis},i}}{M_i} \Delta_i g_i \right) \dot{m}_F \tag{6}$$

in which N_A is the Avogadro constant, $b_{\mathrm{fis},i}$ is the fission exergy of *i-th* fissionable element, Δ_i is the difference of enrichment level of fresh and burnup fuel, M_i is the atomic mass of *i-th* fissionable element, g_i is the mass share of *i-th* fissionable element, and $\dot{m}_F$ is the fuel mass stream, which can be calculated from the above equation:

$$\dot{m}_F = \frac{\dot{Q}_{HTR}}{\left(1 - \xi \dot{Q}_{HTR}\right) W_F \frac{86400s}{d}} \tag{7}$$

in which $\dot{Q}_{HTR}$ is the high temperature nuclear reactor thermal capacity, $\xi \dot{Q}_{HTR}$ is the heat loss in a high temperature nuclear reactor, W_F is the nuclear fuel burnup level, d is the number of work days, and $86400s$ is number of the seconds. The difference in enrichment levels of fresh and burnup fuel for fuel composed only of U_{235} can be estimated from the equation:

$$\Delta_{U235} = \frac{M_{U235} W_F \frac{86400s}{d}}{N_A \cdot 1.60217662 \cdot 10^{-16} e_{\mathrm{fis},U235}} = 0.0842 \tag{8}$$

in which M_{U235} is the atomic mass of U_{235} and $e_{\mathrm{fis},U235}$ is the fission energy of U_{235}.

The exergy destruction rate (exergy losses) in the turbomachinery, for example, in the vapor turbine of GT (RI)-ORC can be expressed:

$$\begin{aligned} \delta \dot{B}_{VT-11} &= \dot{m}_{1001} \left(b_{1001} - b_{1101}\right) \\ &= \dot{m}_{1001} \left[\left(h_{1001} - h_{1101}\right) \eta_m \eta_{el} \right. \\ &\qquad \left. - T_0 \left(s_{1001} - s_{1101}\right)\right] \end{aligned} \tag{9}$$

The cycle net electric efficiency $\eta_{el,net}$ refers to the value of the cycle's electrical power to the capacity of the nuclear reactor increased by heat losses in the reactor:

$$\eta_{el,net} = \frac{N_{el,net}}{\dot{Q}_{HTR}} \left(1 - \xi \dot{Q}_{HTR}\right) \tag{10}$$

2.2. Main dimensions of a fluid-flow machinery

The key aspect of this study was to compare the machinery size of the proposed power cycles. The idea of a modular design of a nuclear power plant was aimed at decreasing the time and construction costs. Second, smaller power units are generally more flexible in terms of start-ups and power load changes. Small sizes limit the surfaces loaded by working fluid pressure, which allows for thinner hydraulic construction walls. This feature is particularly important in the new models of RES-based power systems. In the paper heat transfer surface area and last-stage blades length of the turbines were investigated.

Calculation of heat transfer surfaces are based on simplified model of overall heat transfer proposed by Peclet [30]:

$$\dot{Q} = kS\Delta\bar{T} \tag{11}$$

in which $\dot{Q}$ is the heat transfer rate, S is the surface of heat flow, and k is the overall heat transfer coefficient as shown in Table 3, $\Delta\bar{T}$ is the logarithmic temperature difference:

$$\Delta\bar{T} = \frac{\Delta T_A - \Delta T_B}{ln\frac{\Delta T_A}{\Delta T_B}} \tag{12}$$

in which ΔT is the temperature difference between heated and heating fluid at the inlet to the heat exchanger A and outlet B.

The overall HTC for each fluids in engineering applications varies over a wide range, as it depends on the type of exchanger, materials and thermodynamic properties of the fluids. In this analysis, the following assumptions were made for the selection of the HTCs, in accor-

Table 3
Approximate overall heat transfer coefficient for chosen fluids in common engineering applications [31].

Heating medium	Heated medium	Heat transfer coefficient *k*, W/(m ^{2}K)
Helium	Helium	1200
Helium	Water steam	1200
Helium	Water (boiling)	2000
Helium	Water	1200
Helium	Ethanol vapor	1000
Helium	Ethanol (boiling)	1700
Helium	Ethanol liquid	1000
Helium	Ammonia vapor	1000
Helium	Ammonia (boiling)	1700
Helium	Ammonia liquid	1000
Water steam (condensation)	Water	3000
Ethanol vapor (condensation)	Water	2000
Ammonia vapor (condensation)	Water	2000

dance with the heat exchanger design principles [31]:

- the HTC for water is higher than for selected low-boiling points fluids;
- the same values of HTC were adopted for ammonia and ethanol because their ranges overlap.

Nevertheless, the adopted values are indicative and it is therefore beneficial to carry out preliminary designs of appropriate heat exchangers and compare the results with those proposed in Table 2. In case of discrepancies, new values of nominal conditions may be determined based on the power of the exchangers shown in section 3.3 and the parameters of the working fluids at the characteristic points of cycles (see Appendix).

Analysis of the data gathered for Table 3 leads to the conclusion that SRC provides higher heat transfer coefficients than ORC, which leads to smaller heat transfer surfaces. However, condensation of steam at 33 °C requires a 95% vacuum (0.05 bar), which leads to high specific volume and larger turbomachinery sizes. This issue for water and low-boiling point fluids is addressed in the work of Kowalczyk et al. [20] and Ziółkowski et al. [21].

A comparison of ORC and SRC turbines is based on the assumption that the velocity of working fluid at the turbine outlet remains constant for each cycle. During the preliminary design of steam turbines, this velocity is usually assumed as $v = 250 - 300\ m/s$ [28]. According to Fig. 9, the last-stage free-flow area (A) is a turbine stage cross-sectional area between the turbine blades:

$$A = D\pi L\tau \tag{13}$$

In which L is the turbine stage blades length, D is the stage pitch diameter, and τ is the cross-sectional free area coefficient, resulting from the blade thickness.

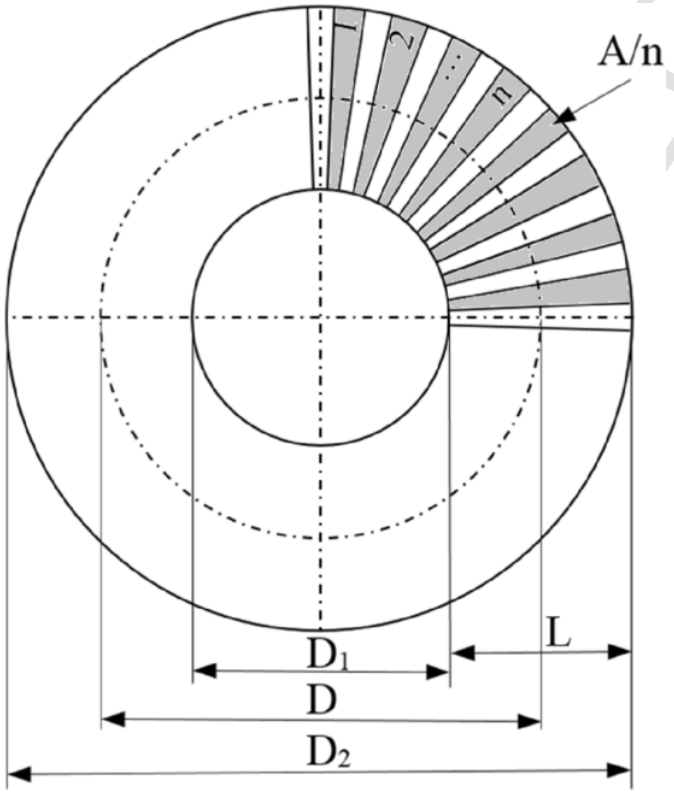

Fig. 9. The last-stage free-flow turbine area. A: last turbine stage cross-sectional area, n: blade number, L: turbine stage blade length, D: stage pitch diameter, D_1: diameter at the root of rotor blade, D_2: diameter at the rotor blade tip.

In this study, the pitch diameter D and the coefficient τ were assumed to be constant for each turbine. The pitch diameter results from the expanding gas velocities and the shaft rotation speeds. The correlation is included in the so-called turbine stage speed triangle, whereas the coefficient results from the turbine blade number and thickness. Employing this assumption, the last-stage turbine blade length is directly proportional to the volumetric flow rate $\dot{V}$, according to the formula:

$$A = \frac{\dot{V}}{v} = D\pi L\tau \tag{14}$$

The free-flow area limits the working fluid flow rate. It is a function of the working fluid volume flow rate, shaft rotation speed, and blade material tensile strength. Large values of free-flow area require long blades made of materials, such as titanium, with high tensile strength, few double-flow LP turbine cylinders, or a decrease in rotation speed of the shaft. Each of these solutions negatively affects the initial cost of the power plant. On the other hand, if turbine blades are too short, they need to be fixed on smaller pitch diameter. This requirement imposes higher rotation speeds to meet requirements on the stages speed triangle. Rotation speeds >3000 RPM are not recommended in 50 Hz systems because these turbines require gearboxes or electric inverters. Moreover, blade material and fixing must withstand higher tensile forces.

3. Results

The results are divided into four subsections. The thermodynamic properties of working fluids are characteristic points of investigated cycles for optimal configurations and are presented in the Appendix.

3.1. Power and energy efficiency

Values of power and energy efficiency were obtained as a result of the optimization process. The main optimization manner in cases of gas and combined cycles is pressure rationing in the Joule–Brayton cycle. This parameter affects the gas turbine outlet temperature and therefore, also the bottoming turbine inlet temperature. Results of pressure ratio optimization are presented in Fig. 10. Dots denote the gas turbine pressure ratio for which the reactor inlet temperature is around 450°

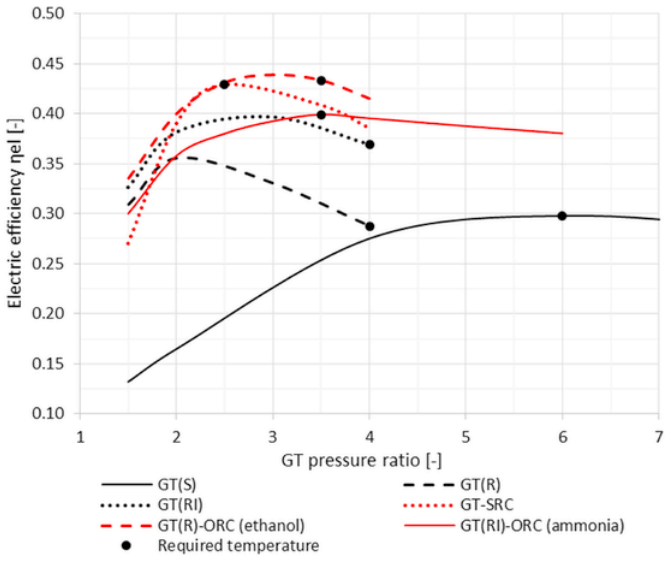

Fig. 10. Electrical efficiency of investigated thermodynamic cycles in GT pressure ratios. Dots indicate the proper inlet temperature for the HTR. GT(S): simple closed gas turbine cycle, GT(R): the gas turbine cycle with heat regeneration, GT (RI): gas turbine cycle with heat regeneration and intercooler.

C. The reactor inlet temperature depends mainly on the core and fuel design and strongly affects the reactor exergy efficiency. For higher inlet temperature, larger streams of cooling gas are necessary, which increase the size of the fluid-flow machinery. For comparative analysis, this value was held at a constant value with a tolerance of ±25K.

The most energy efficient cycle is the GT (RI)-ORC with an energy efficiency of 43.88%. However, in the most efficient configuration, the HTR inlet temperature of cooling helium is too high (518°C). For assumed HTR inlet temperatures, the energy efficiency drops to 43.33%. The second cycle is the GT-SRC, which achieves a 42.86% energy efficiency. The bottoming cycle with ammonia reaches 39.90% energy efficiency. The most efficient gas turbine cycle is the GT (RI), which reaches 39.66% efficiency; however, the reactor inlet temperature exceeds 600°C. For temperatures around 450°C, the energy efficiency decreases to 36.90%. Taking into account the HTR inlet temperature, this value is > 6 pp higher than for the simple Joule–Brayton cycle and cycle with heat recovery.

Use of standard gas cycle modifications, such as heat regeneration and intercooling, influences not only the energy efficiency of the cycle and working fluid temperatures but also the power ratio of the gas and bottoming cycle. Table 4 contains electrical power and energy efficiency in net electricity generation related to reactor thermal capacity in the Joule–Brayton, bottoming, and combined cycles.

Adding a bottoming cycle to the gas turbine cycle increases the energy conversion efficiency and complicates the cycle. Power generation in the gas cycle decreases because high temperature of flue gases is needed. However, use of low-boiling point fluids reduces this effect since this kind of working fluid achieves higher cycle efficiencies for lower temperature heat regeneration, intercooling in the gas cycle become advantageous. Application of heat regeneration and intercooling in the gas cycle with ammonia as a working fluid in the bottoming cycle caused an increase in the gas cycle electric power generation from 73.55 to 152.26 MW compared to GT-SRC and caused a decrease in the power of the bottoming cycle from 156.21 to 87.14 MW. The cycle energy efficiency decreased in this case by 3.14 pp.

During the optimization process, two more parameters were investigated: (1) cooling of helium in the HE-05 and -08 coolers at the VG-04 and -07 vapor generator outlets. This improvement negatively affected the efficiency; however, the cooling also caused a decrease in the temperature at the HTR inlet. In case of ethanol the efficiency dropped from 43.33% to 40.27%, and the temperatures decreased from 518 to 476 °C and (2) in the intercooling case, the compressor pressure ratio was optimized. For open gas turbine cycles, the pressure ratio in both compressors is equal to ensure the highest cycle efficiency [32]. In the case of the bottoming cycle, it was selected to align the enthalpy increase in both the VG-04 and -07 vapor generators, which offered the highest energy efficiency of the combined cycle.

Table 4
Power and energy efficiency of analyzed thermodynamic cycles.

Cycle	Joule–Brayton cycle power $N_{el,GT}$ MW_{el}	Bottoming cycle power $N_{el,ORC/SRC}$ MW_{el}	Overall	
			Power $N_{el,net}$ MW_{el}	Energy efficiency $\eta_{el,net}$ %
GT	180.53	–	180.53	29.79
GT(R)	174.22	–	174.22	28.74
GT(RI)	221.39	–	221.39	36.90
GT-SRC	73.55	183.62	257.17	42.86
GT(R)-ORC (Ethanol)	103.18	156.78	259.96	43.33
GT(RI)-ORC (Ammonia)	152.26	87.14	239.40	39.90

3.2. Exergy loss analysis

The exergy analysis is based on the Second Law of Thermodynamics. It indicates loss of available energy, which could have been converted into work, had an ideal thermodynamic process been employed. The exergy analysis is a powerful tool. In Ref. [33], an exergy analysis was used to compare different configurations of the modernization of a gas-steam CHP plant. While the reduction of heat output of a CHP plant significantly reduces the energy efficiency of the facility, the exerted efficiency was maintained at a similar level. In works of Stanek et al. the exergy analysis was used to analyze the thermo-ecological cost, in terms of the whole life cycle chain, for hard coal [34] and nuclear power plant [35]. The results showed that the thermo-ecological cost of using a given energy source is significantly influenced by the stage of extraction, transport and fuel preparation. This aspect is often neglected in energy analyses of power plants.

In this paper authors employ the exergy analysis to determine the losses in individual devices of the cycles. Such an approach makes the influence of cycle modifications on the energy conversion efficiency more transparent. Results of the exergy destruction rate analysis are presented in Fig. 11. Additionally, values from Fig. 11 are presented in Table 5.

The highest exergy destruction rate occurred in the reactors. Those losses resulted from large differences between the exergies of fission and helium increase in the core. In practice, large temperature differences between fuel elements and cooling medium occurs. The second largest source of exergy destruction are helium coolers during the GT (RI) cycle. In this device, large temperature differences between helium and cooling water occur. Application of bottoming cycle can lessen those losses by approximately 5-times, thanks to low condensation temperatures. Small exergy destruction in the condensers and high destruction in the reactor are opposite to energy cycles in which the largest losses occur in condensers and the smallest in reactors. The ORC bottoming cycle causes a decrease in the exergy destruction rate in the regenerative heat exchanger; however, it brings new losses in the vapors generators. The ethanol vapor generator imposes lower exergy destruction rates than ammonia or steam generators because of ethanol's supercritical state and small temperature differences between helium and ethanol along with the whole heat exchange process. The most efficient cycle (the GT-SRC) generates the largest exergy destruction rate in the steam generators; however, it causes the lowest gas turbine and compressor exergy destruction.

Analysis of equation (4) indicates that the exergy destruction rate occurs even in adiabatically-insulated heat exchangers and results from the temperature differences between heating and heated medium. Therefore, the exergy destruction rate will decrease if the temperature difference becomes smaller. The phenomena of exergy destruction during heat exchange can be easily explained using heat transfer diagrams representing temperature of heated and heating media in functions of exchanged heat Qx related to overall heat Q exchanged in the device. This issue is discussed in subsection 3.4.

3.3. Heat transfer surface area and the last-stage blades length

The power plant cubature affects investment costs in two ways. Firstly, large machinery needs more production material and work. Second, if the machinery is small enough, it can be constructed in a modular design. Because the analysis assumes usage of a modular nuclear reactor, it is preferred to propose also other parts of the plant in a modular design to limit investment costs.

The amount of waste heat flow rate in the GT cycle was 421.26 MW and was emitted to the environment in the HE-04 heat exchanger. Using simplified approach (subsection 2.2), the heat transfer surface area was estimated as 2973 m^2. In the cycle with heat regeneration and intercooling GT (RI), heat rate of losses was reduced to 369.35 MW

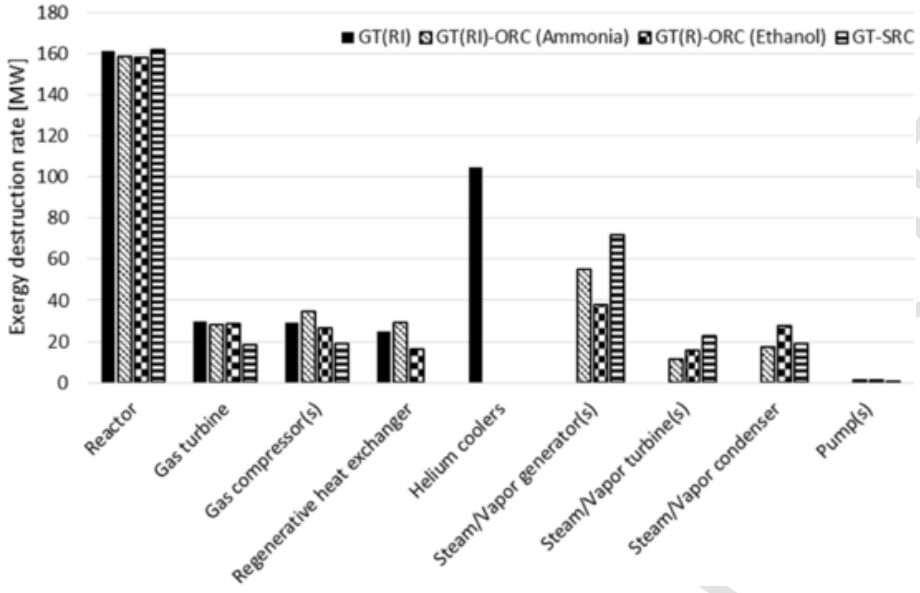

Fig. 11. Exergy destruction rate in each component of the thermodynamic cycles.

Table 5
Exergy destruction rate in cycle components under nominal loads.

	Exergy destruction rate, MW			
	GT (RI)	GT (RI)-ORC (Ammonia)	GT(R)-ORC (Ethanol)	GT-SRC
Reactor	161.22	158.38	157.89	161.54
Gas turbine	29.99	28.35	28.65	18.61
Gas compressor(s)	29.08	34.69	26.53	18.92
Regenerative heat exchanger	24.79	29.44	16.21	–
Helium coolers	104.81	–	–	–
Steam/Vapor generator(s)	–	55.12	37.66	72.00
Steam/Vapor turbine(s)	–	11.18	15.55	22.86
Steam/Vapor condenser	–	17.54	27.80	18.97
Pump(s)	–	1.39	1.27	0.22
Total	349.89	336.09	311.56	313.12

Table 6
Heat exchanger transfer rates for nominal HTR load for the most energy efficient cycles.

	Heat exchanger transfer rate, MW			
	GT (RI)	GT (RI)-ORC (Ammonia)	GT(R)-ORC (Ethanol)	GT-SRC
Regenerative heat exchanger	317.35	342.23	53.27	–
Helium coolers	369.35	–	–	–
Steam/Vapor generator(s)	–	431.67	486.79	519.31
Steam/Vapor condenser	–	334.76	318.45	324.80
Total	686.70	1108.66	1674.14	544.10

Table 7
Heat exchanger surface area comparison.

	Heat exchanger surface area, m^2			
	GT (RI)	GT (RI)-ORC (Ammonia)	GT(R)-ORC (Ethanol)	GT-SRC
Regenerative heat exchanger	7220	6643	1110	–
Helium coolers	4105	–	–	–
Steam/Vapor generator	–	12020	10867	5101
Steam/Vapor condenser	–	10740	9337	8751
Total	11326	29403	21315	13852

and was divided between the HE-04 and -06 coolers (210.70 and 158.66 MW, respectively). Use of heat regeneration requires an additional heat exchanger (HE-03) with a heat transfer rate of 317.35 MW, which caused a total increase of heat transfer surface by 243% in the GT cycle. Moreover, additional heat exchangers cause an increase in pressure losses in the helium loop, which caused a decrease in gas turbine expansion ratio. Conversion of the GT into GT (RI) with heat regeneration and intercooling between compressor stages required 381% increase in heat transfer surface area from 2973 to 11326 m^2. The heat exchangers' transfer rates and surface area in the most energy efficient cycles are presented in Tables 6 and 7. The results are consistent with heat transfer coefficients shown in Table 3. Pressure, mass and volumetric flow rates at inlets and outlets of the turbines are presented in Table 8.

Comparing the two most efficient bottoming cycles, the GT(R)-ORC (ethanol) and GT-SRC were characterized by the smallest heat transfer areas. The heat transfer surface area of the ammonia cycle was about 212% larger than for the SRC. In case of ethanol cycle, the surface area was only 54% larger. As previously described, in both ORCs, the helium coolers were suppressed to improve the cycle's energy efficiency in order to increase the total heat transfer surface area by 260%, the GT(R)-ORC (ethanol) by 88%, and the GR-SRC by 22%.

Besides increasing the heat exchanger sizes, the bottoming cycles impose new turbines into the thermodynamic cycles. In the case of the GT-SRC, regarding to the live steam parameters of 572 °C and 142.5 bar, and on the basis of existing steam power plants [28], the steam turbine is proposed as a conventional three cylinder turbine with a high-, intermediate-, and low-pressure parts. Total power output of the steam turbine was 183.62 MW. It was assumed that the low-pressure turbine was a double flow unit with a last-stage blade length

Table 8
Pressures, masses, and volumetric flow rates of selected working fluids.

Cycle	Cycle point	Pressure, bar	Mass flow rate, kg/s	Volumetric flow rate, m^3/s	Cycle point	Pressure, bar	Mass flow rate, kg/s	Volumetric flow rate, m^3/s
GT-SRC	0402	142.5	57.61	1.45	1201	0.05	137.58	3778.19
GT(R)-ORC (Ethanol)	1001	171.0	297.01	1.86	1101	0.12	297.01	1669.40
GT (RI)-ORC (Ammonia)	1001	211.0	320.51	3.63	1101	12.70	320.51	30.23

of 800 mm. According to equation (14), both ORC turbines were significantly smaller. The volumetric flow rate at the ethanol turbine outflow is 44.19% of the steam unit outflow. This allowed for a decrease in the last-stage blade length to about 700 or 350 mm in the corresponding single or double flow low-pressure turbine. With ammonia, the volumetric flow rate is almost 120 times smaller than steam, which required turbine redesign. However, ammonia turbines could be designed as single cylinder units because volumetric flow increase across the turbine is only about 9 times, which is a great advantage in terms of modular designs of power plants and decreases in construction costs.

Despite issues concerning the last-stage dimensions, an important issue is also the first stage blade length. Very small volumetric flow rates cause problems with very short blades. In cases of small-scale ORC turbines, the solution is to increase rotation speeds; however, this increase imposes problems with the electrical generator (See Żywica et al. [36]). Another innovative approach proposed by Kosowski et al. [37] assumes the part flow through all five axial stages of the micro turbine. This idea allows for construction of highly efficient turbines with small inlet volumetric flow that can be adopted for large-scale units. However, the volumetric flow at the turbine inlet in both ORCs was higher than with steam, so there was no need for application of a high-rotation speed turbine. Additionally, in work [38] the energy efficieny of solo SRC is compared with solo closed Joule–Brayton cycle for HTR operation. The SRC large-scale unit achieves 4.6 - 8.2 pp. higher efficiency than gas turbine cycle, depending on the cycles parameters.

3.4. Partial load performance

Currently, for many thermal power plants, the partial load operation covers the largest part of the year. The possibility of lowering the minimal load becomes the most important operating aspect. However, the partial load operation should ensure the highest possible energy conversion efficiency at the same time. According to work of Xu et al. [29], safe and stable minimal thermal HTR loads can be reduced to 30% of nominal loads.

Changes in nuclear reactor thermal capacities require an adjustment in gas and bottoming cycle thermodynamic parameters. Reduction of heat transfer rate supplied into the Joule–Brayton closed cycle indicates the need for mass flow rate reduction of the working medium if constant temperature at the reactor outlet is to be maintained. In the open gas cycle, throttling of the working fluids or reduction of compressor rotation speeds is required to reduce mass flow rate. Both of the above-mentioned methods reduce the compression ratio in the cycle and reduce expansion in the turbine, which causes an increase in exhaust temperatures and decreases the efficiency of electric power generation. In closed gas cycles, it is possible to adjust the mass flow rate by changing the gas pressure in the loop without changing the compression ratio. This method affects only the gas density and maintains the cycle's thermal and flow efficiency. For partial loads, helium pressures can be adjusted to maintain constant volumetric flow rate at the reactor outlet to about 100 m^3/s. For nominal loads, the maximum pressure in the cycle, at the GC-09 compressor outlet, is 65 bar. For 30% of the HTR nominal load the pressure is 19.5 bar. The reduction in helium pressure only caused an increase in entropy, while the temperatures distribution on the cycle was constant as shown in temperature-specific entropy diagram (Fig. 12) with the GT-SRC example.

It can be assumed that power governing is based on the sliding pressure control. This control provides the most energy efficient method of steam turbine governing in which one turbine operates with one boiler in a so-called block system. This method manages power adjustments by the feed water pumps rotation speed control. A decrease in pump rotation speed causes a decrease in boiler water mass flow and pressure. Next, fuel mass flow rate was adjusted to maintain the temperature of live and reheated steam if reheating is applied. Obviously, this type of governing system is characterized by a relatively long response time, so it must be supported with a throttle or nozzle governing system to protect the power system from the rapid frequency changes.

The relationship between mass flow rate through the turbine and the live steam/vapor pressure is defined by the Stodola's cone law [28]. This relationship takes on a linear function for condensing turbines. Values of flow rates in live steam pressure functions measured on the 18K360 steam turbine are shown in Fig. 13.

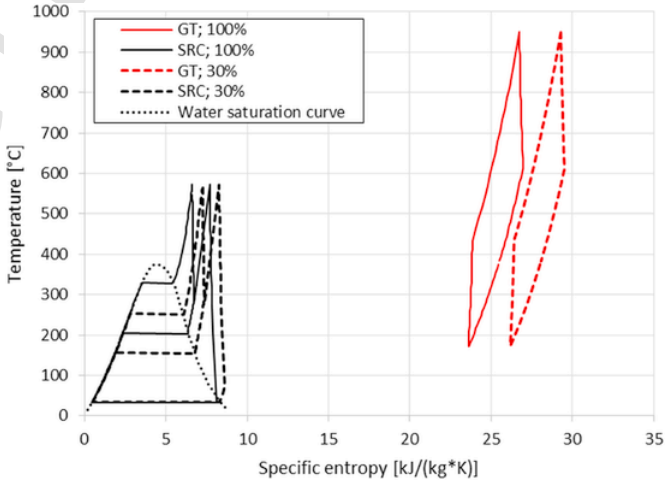

Fig. 12. Temperature-specific entropy diagram of the GT-SRC for full and partial HTR loads. The cycle follows the scheme in Fig. 4.

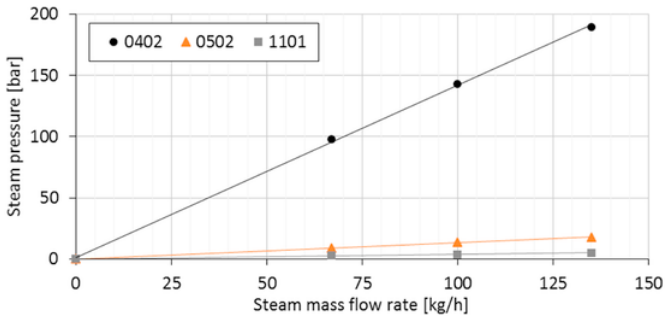

Fig. 13. Pressure distribution at the high-, intermediate-, and low-pressure turbines according to Stodola's cone law (linear functions) and measurements on the 18K360 steam turbine using points of GT-SRC from Fig. 7.

SRC consists of a subcritical steam cycle, so a decrease in boiler pressure mainly affects the low-pressure turbine outlet temperature. As is shown in Fig. 12 for nominal loads, the turbine outlet steam is wet, while under 30% of the HTR thermal load, the steam is slightly superheated. Issues of possible ventilation at the last-stage of the low-pressure turbine was not addressed in this paper. The second effect of feed water pressure decrease is a change in steam generator operation conditions., namely, lower pressures cause lower evaporation temperatures, which causes an increase in vaporization enthalpy and temperature difference between helium and water/steam. This phenomenon is shown in Figs. 14 and 15 on the heat transfer charts representing temperatures of heated and heating media in exchanged heat Qx related to overall heat transfer Q exchanged in the SG-04 and -07 steam generators, respectively. The helium line concurrently presents nominal and partial loads because there are no temperature changes in the helium loop under partial loads.

As mentioned previously, this phenomenon caused a decrease in energy efficiencies of the cycles via exergy destruction during heat transfer. Under nominal HTR loads, exergy destruction in the SG-04 and -07 were 36.63 and 30.89 MW, respectively. For the 30% HTR load, losses were 12.65 and 12.54 MW, respectively. These losses were 6.11% and 5.15% of the actual HTR thermal capacity of the SG-04 and -07 nominal loads, respectively. Under a 30% HTR load, these losses increase to 7.03% and 6.97% of the actual HTR thermal capacity. It should be noted that pinch temperatures in SG-07 were limited by an assumption of 15 K, but in the SG-04 case, it was result of the optimization process and was limited by cyclic energy balance.

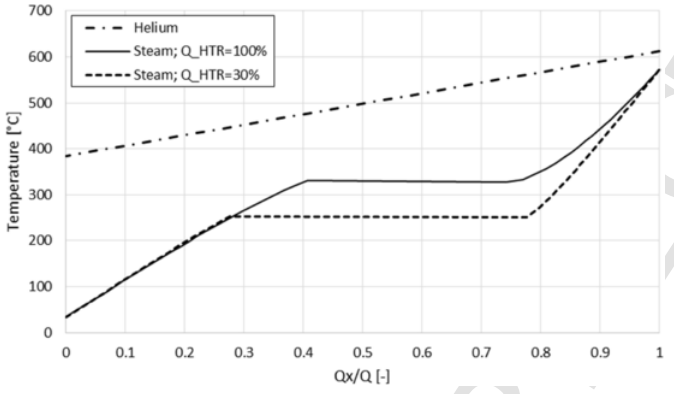

Fig. 14. Temperature of heating and heated medium in exchanged heat Qx related to overall heat Q exchanged in the SG-04 steam generator in GT-SRC. The outlet nominal pressure of steam was 142 bar.

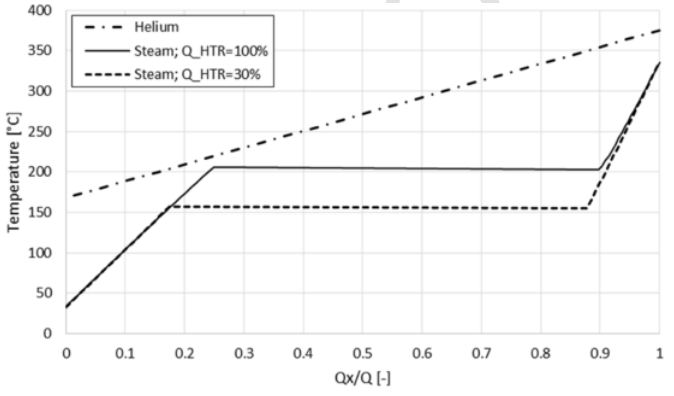

Fig. 15. Temperatures of heating and heated medium in exchanged heat Qx related to overall heat Q exchanged in the SG-07 steam generator in GT-SRC. The outlet nominal pressure of steam was 19 bar.

3.4.1. Influence of ORC cycle on heat transfer

In case of the ORC with ethanol as a working fluid, the vapor at the turbine outlet was superheated under both partial and nominal loads (Fig. 5). However, the issue is the supercritical state of the ethanol in the vapor generator. Using sliding pressure to govern the working fluid becomes subcritical under partial loads, which requires appropriate vapor generator design. Second, the exergy destruction was more significant due to a larger temperature increase in differences between helium and ethanol. Therefore, two approaches were investigated. The first one used only the sliding pressure governing, while the second one combined sliding pressure and throttling governing. In the second approach, ethanol was under supercritical conditions even under minimal load because sliding pressure operated only in the supercritical pressure range. Above the minimal mass flow provided by sliding pressure, the throttling governing was used.

In Fig. 16, the heat transfer chart represents temperatures of heated and heating media in exchanged heat Qx related to overall heat transfer Q exchanged in the VG-04 vapor generator for nominal and minimal cycle loads. The dotted curve was named "Ethanol; Q_HTR = 30%, subcritical" refers to sliding pressure, and the dashed curve "Ethanol; Q_HTR = 30%" refers to combined sliding pressure and throttling governing.

The energy efficiency of the cycle for nominal load was 43.33%. Under minimal loads, the cycle reached 41.27% and 40.89% using sliding pressure and combined governing, respectively. For nominal loads, exergy destruction in the VG-04 was 37.66 MW (6.28% of the actual HTR thermal capacity). For the 30% HTR load, the exergy destruction was 11.74 MW (6.52%) and 13.53 (7.53%) for combined and sliding pressure governing, respectively. The cycle energy efficiency was higher in case of sliding pressure despite the higher exergy destruction in the vapor generator because additional exergy destruction, equal to 2.78 MW (1.54%), occurred in the control valve after using combined governing.

The GT (RI)-ORC with ammonia was the most sensitive cycle for the governing method. In Fig. 17, the heat transfer chart represents temperatures of heated and heating media in exchanged heat Qx related to overall heat Q exchanged in the VG-04 for nominal and minimal cycle loads. The VG-07 works under the same conditions. The dotted curve was named "Ammonia; Q_HTR = 30%, subcritical" refers to sliding pressure governing, the dashed curve "Ammonia; Q_HTR = 30%" refers to combined sliding pressure and throttling governing.

For ammonia, changes in temperature distribution along the heat exchanger were greater than with ethanol. The energy efficiency of the cycle for nominal loads was 39.90%. Under minimal loads, the cycle reached 35.82% and 34.00% using sliding pressure and combined governing, respectively. For nominal loads, exergy destruction in the VG-

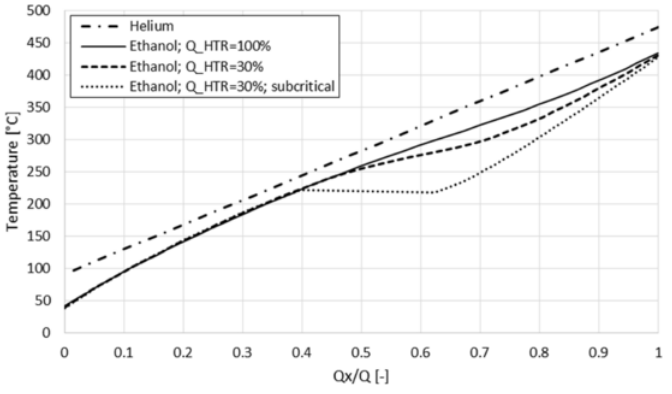

Fig. 16. Temperatures of heating and heated medium in exchanged heat Qx related to overall heat Q exchanged in the VG-04 vapor for ethanol under supercritical conditions in GT(R)-ORC. The outlet nominal pressure of ethanol was 171 bar.

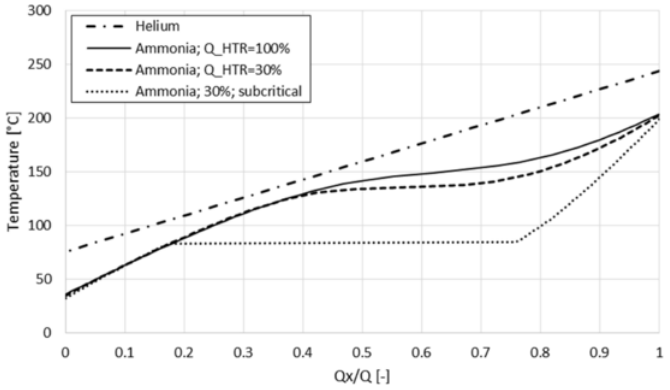

Fig. 17. Temperature of heating and heated medium in exchanged heat Qx related to overall heat Q exchanged in the VG-04 and -07 generators for ammonia under supercritical conditions in GT (RI)-ORC. The outlet nominal pressure of ammonia was 228 bar.

04 was 27.05 MW (4.51% of the actual HTR thermal capacity). For the 30% HTR load, exergy destruction was 8.53 MW (4.74%) and 11.94 (6.64%) for combined and sliding pressure governing, respectively. The cycle energy efficiency is higher in cases of sliding pressure despite higher exergy destruction in the vapor generator because additional exergy destruction, equal to 10.75 MW (5.97%), occurred in the control valve using the combine governing.

3.4.2. Influence of ORC cycle governing on the turbine

Low vapor pressure under minimal loads also caused an increase in turbine outlet temperatures. Under HTR full load the ammonia dryness fraction at the turbine outlet equals 0.92, for minimal load the steam is superheated to 57 °C for combined governing and up to 93 °C for sliding pressure governing. The temperature-specific entropy chart in Fig. 18 presents the ammonia cycle under full and minimal loads using sliding pressure and combined governing. As previously mentioned, sliding pressure caused subcritical ammonia pressure at the pump outlet, which affects heat exchange in vapor generators. However, vapor generators designed to withstand those operating conditions would be efficient solution. Moreover, under minimal loads, heat rates of precooling ammonia at temperatures ranging from 93 to 31 °C at the condenser inlet equaled 14.32 MW, which could be utilized for heating purposes.

Table 9 presents the cycle's thermodynamic performance for minimal reactor load equal to 30% of its nominal thermal capacity.

The partial load analysis indicates that under minimum loads, the most efficient cycle is the GT(R)-ORC with ethanol. As was previously mentioned, before the closed-loop helium cycle energy efficiency is independent of load. Therefore, decreasing the energy efficiency of the combine cycle results from the bottoming cycle governing. The highest energy efficiency under partial loads were achieved using sliding pressure governing. In cases of GT(R)-ORCs, efficiency decreases for 30% HTR thermal load is at least 2.06 pp. The same value was attained in the case of SRC. In cases of ethanol and combined governing, which maintained supercritical conditions in the vapor generator under partial loads, the energy efficiency dropped by 2.44 pp. In the cases of the ammonia cycle, the energy efficiency under minimal load dropped by 4.08 and 5.90 pp for sliding pressure and combined governing, respectively. For future analyses, nozzle instead of throttle governing should be considered; however, this method can affect the high-pressure turbine isentropic efficiency.

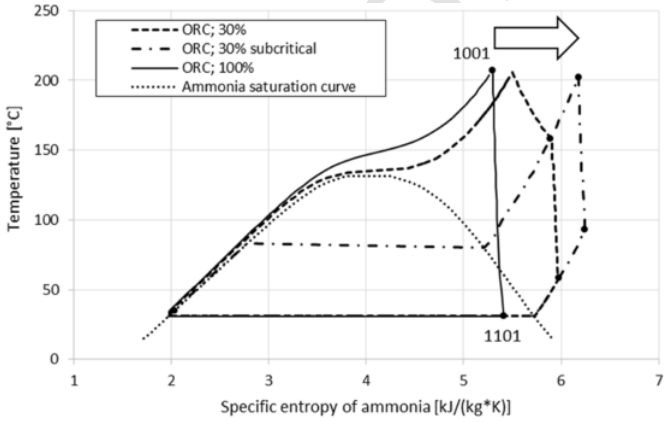

Fig. 18. Temperature-specific entropy diagram of the bottoming cycle of the GT (RI)-ORC for full (ORC; 100%) and partial HTR loads using sliding pressure (ORC; 30%; subcritical) and combined governing (ORC; 30%). The cycle progressed according to the scheme in Fig. 4.

Table 9
Power output and energy efficiency for 30%-loaded HTR.

Cycle	Joule–Brayton cycle power output $N_{el,GT}$ MW_{el}	Bottoming cycle power output $N_{el,ORC/SRC}$ MW_{el}	Overall	
			Power output $N_{el,net}$ MW_{el}	Energy efficiency $\eta_{el,net}$ %
GT-SRC	24.16	49.19	73.44	40.80
GT(R)-ORC (Ethanol), sliding pressure governing	32.32	41.96	74.28	41.27
GT(R)-ORC (Ethanol), combined governing	31.85	41.76	73.60	40.89
GT(RI)-ORC (Ammonia), sliding pressure governing	46.35	14.85	61.20	34.00
GT(RI)-ORC (Ammonia), combined governing	47.17	17.31	64.47	35.82

4. Conclusion

This paper presents a comparative study of close loop Joule-Brayton cycle cooling HTR in three configurations: GT, GT(R), GT (RI); and two combined cycles with bottoming cycles: GT-ORC and GT-SRC. Moreover, the ORC is analyzed in two configurations GR(R)-ORC and GT (RI)-ORC. Results for three working fluids for bottoming cycles were presented: water, ammonia and ethanol. Working fluid providing the highest energy efficient for the GR(R)-ORC is ethanol, while in the GR (RI)-ORC is ammonia. Thermodynamic parameters for fluid-flow machinery were selected basing on current operated machinery, not on the state-of-the-art design. That is because helium turbomachinery is relatively immature technology. Therefore, it is possible to achieve higher energy efficiency of the cycles, if pressure drops, heat losses will be decreases and isentropic efficiency of turbomachinery increased. However, there is a significant influence of those parameters on the combine cycle configuration.

As the result of optimization process, the GR(R)-ORC with ethanol as a working fluid in the bottoming cycle reached the highest energy efficiency under nominal and minimal HTR loads, equal to 43.33% and 41.27%, respectively. The minimal HTR load was assumed as 30% of it nominal thermal capacity. The SRC achieved 42.86% and 40.89%, respectively, and was the second most energy efficient cycle. Moreover, the heat transfer surface area was only about 22% larger than in case of the GT (RI), while the energy efficiency was 5.96 pp. and 3.99 pp. higher for the nominal and minimal HTR loads, respectively. The

heat transfer surface area in the ethanol cycle was 188% of the GT (RI) surfaces area, while in case of ammonia, it was 260% of the GT (RI).

Both low-boiling point fluids were characterized by lower volumetric flow rate through the last turbine stage, which affected the machinery size. The lowest turbine size and the smallest volumetric flow rate increase at the turbine inlet and outlet provided ammonia. Ammonia was condensed under a pressure of 12.7 bar if ambient temperature was used for cooling. The volumetric flow rate at turbine outflow was only about 8-times larger than at the inlet. Moreover, the volumetric flow rate at the turbine inlet was more than twice larger than steam. Those parameters provided good boundary conditions for turbine design. In contrast, the steam turbines in the steam Rankine cycle were the largest turbine of the analyzed solutions. The volumetric flow rate at the low-pressure turbine outlet was 2606-times larger than at the inlet to the high-pressure part. For that reason, the steam turbine was divided into three cylinders, and the low-pressure part was designed as a double flow unit. Ethanol provides about 2-times shorter last-stage blades, while volumetric flow at the turbine inlet is 28% larger than with steam.

The exergy analysis indicates the highest exergy destruction occurred in the reactors, which was opposite to the energy efficiency, especially if heat losses in the reactor were omitted. The second largest exergy destruction occurred in helium coolers in gas cycles without bottoming cycles. In case of the GT (RI) cycle, it was 104.81 MW. Bottoming cycles caused a decrease in this loss to about 17–28 MW; however, this decrease now causes exergy destruction in steam and vapor generators. The highest exergy destruction in the bottoming cycles occurred in steam generators in the SRC (72.00 MW), the second was the ammonia vapor generator (55.17 MW). The most exergy efficient was the ethanol vapor generator with an exergy destruction of 37.66 MW.

The key features of the bottoming cycles are increases in the energy conversion efficiency; however, properly selected working fluid can also cause a decrease in the size of heat exchangers and turbomachinery. Those features are particularly important in field of energy cycle miniaturization aimed at modular design and prefabrication, which could lead to a decrease in investment costs.

Acknowledgments

This research did not receive any specific grant from funding agencies in the public, commercial, or not-for-profit sectors. Part of this paper has been conducted within the frame of statutory research of the Institute of Fluid Flow Machinery Polish Academy of Sciences. However, the other part of work has been prepared within the frame of statutory research of the Department of Energy and Industrial Apparatus, Faculty of Mechanical Engineering, Gdansk University of Technology.

Appendix.

Tabele A-1
Thermodynamic properties of working fluids in characteristic points of investigated cycles under nominal load.

Cycle	Cycle point	Fluid	T[°C]	p[bar]	s [kJ/(kg*K)]	i[kJ/kg]
GT (RI)	0101	helium	950	58.66	26.91	6374
	0201	helium	482	14.67	27.28	3930
	0301	helium	213	13.93	25.1	2536
	0401	helium	35	13.24	22.84	1610
	0501	helium	169	29.78	23.03	2312
	0601	helium	35	28.29	21.26	1614
	0701	helium	173	65.00	21.46	2344
	0302	helium	442	61.75	24.02	3737
GT (RI)-ORC	0101	helium	950	58.66	26.91	6374
	0201	helium	517	16.76	27.24	4111
	0301	helium	244	15.92	25.14	2695
	0401	helium	76	14.33	23.32	1820
	0501	helium	76	14.33	23.32	1820
	0601	helium	251	35.83	23.53	2738
	0701	helium	76	32.24	21.63	1826
	0801	helium	76	32.24	21.63	1826
	0901	helium	204	65.00	21.81	2502
	0302	helium	472	61.75	24.23	3891
	0402	ammonia	204	147.00	5.26	1820
	0702	ammonia	211	147.00	5.33	1853
	1101	ammonia	33	12.70	5.43	1548
	1201	ammonia	33	12.70	2.00	499
	1301	ammonia	38	150.00	2.02	526
GT(R)-ORC	0101	helium	950	58.66	26.91	6374
	0201	helium	517	16.76	27.24	4111
	0301	helium	475	15.92	27.06	3893
	0401	helium	91	14.33	23.54	1900
	0501	helium	91	14.33	23.54	1900
	0601	helium	91	14.33	23.54	1900
	0701	helium	91	14.33	23.54	1900
	0801	helium	91	14.33	23.54	1900
	0901	helium	434	65.00	23.85	3699
	0302	helium	477	61.75	24.26	3917
	0402	ethanol	435	171.00	4.55	1924
	0702	ethanol	–	–	–	–
	1101	ethanol	113	0.12	4.67	1334
	1201	ethanol	33	0.12	1.28	281
	1301	ethanol	37	180.00	1.29	308
GT-SRC	0101	helium	950	61.75	26.8	6375
	0201	helium	613	24.70	27.03	4612
	0401	helium	384	23.46	25.58	3424
	0501	helium	351	23.46	25.32	3253
	0601	helium	375	23.46	25.52	3380
	0701	helium	168	22.29	23.62	2303
	0801	helium	436	65.00	23.87	3707
	0402	water	573	142.50	6.63	3518
	0901	water	279	18.00	6.74	2980
	0502	water	573	17.10	7.71	3631.76
	1101	water	388	5.00	7.76	3248
	1201	water	33	0.05	8.19	2498
	1301	water	33	0.05	0.48	138
	1401	water	33	20.00	0.48	140
	0702	water	335	19.00	6.93	3107
	1601	water	34	150.00	0.48	155

References

[1] V Nian, S Zhong Economic feasibility of flexible energy productions by small modular reactors from the perspective of integrated planning. Prog Nucl Energy 2020;118:103106. doi:10.1016/J.PNUCENE.2019.103106.
[2] M Hussain, F Reitsma, M H Subki, H Kiuchi Advances in small modular reactor technology developments. Vienna: IAEA; 2018.
[3] A Rising World nuclear performance Report 2019. 2019. London.
[4] T Kowalczyk, J Badur Energy and exergy analysis of a gas-vapor cycle topped with a high temperature nuclear reactor heating a termochemical cycle for hydrogen production. Proc. ECOS 2016;1–10. Katowice: 2016.
[5] T Kowalczyk, J Badur, M Bryk Energy and exergy analysis of hydrogen production combined with electric energy generation in a nuclear cogeneration cycle. Energy Convers Manag 2019. doi:10.1016/j.enconman.2019.111805.
[6] J Dewulf, G Van der Vorst, K Denturck, H Van Langenhove, W Ghyoot, J Tytgat, et al. Recycling rechargeable lithium ion batteries: critical analysis of natural resource savings. Resour Conserv Recycl 2010;54:229–234. doi:10.1016/j.resconrec.2009.08.004.
[7] X L Yan, R Hino, editors Nuclear hydrogen production handbook. Boca Raton: CRC Press; 2016. doi:10.1201/b10789.
[8] E Nonbel Description of the advanced gas cooled type of gas cooled reactor (AGR). Roskilde: Riso National Laboratory; 1996.

[9] T Kowalczyk, J Głuch, P Ziółkowski Analysis of possible application of high-temperature nuclear reactors to contemporary large-output steam power plants on ships, 23. Polish Maritime Research; 2016. doi:10.1515/pomr-2016-0018.
[10] W Stanek, editor Thermodynamics for sustainable management of natural resources, green energy and technology. Cham: Springer International Publishing; 2017. doi:10.1007/978-3-319-48649-9.
[11] P Ziółkowski, J Badur, P J Ziółkowski An energetic analysis of a gas turbine with regenerative heating using turbine extraction at intermediate pressure - brayton cycle advanced according to Szewalski ' s idea. Energy 2019;185:763–786. doi:10.1016/j.energy.2019.06.160.
[12] R Bartnik, A Hnydiuk-Stefan, Z Buryn Thermodynamic and economic analysis of a gas turbine set coupled with a turboexpander in a hierarchical gas-gas system. Energy 2019;190:116394. doi:10.1016/j.energy.2019.116394.
[13] A Rising World nuclear performance Report 2019. London: World Nuclear Association; 2019.
[14] K Kunitomi, S Katanishi, S Takada, T Takizuka, X Yan Japan's future HTR—the GTHTR300. Nucl Eng Des 2004;309–327.
[15] H Sato, X L Yan, Y Tachibana, K Kunitomi GTHTR300—a nuclear power plant design with 50% generating efficiency. Nucl Eng Des 2014;275:190–196. doi:10.1016/J.NUCENGDES.2014.05.004.
[16] A Bejan Advanced engineering thermodynamics. Hoboken: Wiley; 2006.
[17] M Jaszczur, M A Rosen, T Śliwa, M Dudek, L Pieńkowski Hydrogen production using high temperature nuclear reactors: efficiency analysis of a combined cycle. Int J Hydrogen Energy 2016;1:1–11. doi:10.1016/j.ijhydene.2015.11.190.
[18] T Kowalczyk, W Stanek, T Simla Thermo-ecological evaluation of polygeneration nuclear energy cycle for electricity and hydrogen production cooperating with wind power plant. Proceedings of 32nd International Conference ECOS. Wroclaw: 2019;2649–2661.
[19] P Ziólkowski, D Mikielewicz, J Mikielewicz Increase of power and efficiency of the 900 MW supercritical power plant through incorporation of the ORC. Arch Therm 2013;34:51–71. doi:10.2478/aoter-2013-0029.
[20] T Kowalczyk, P Ziółkowski, J Badur Exergy analysis of the Szewalski cycle with a waste heat recovery system. Arch Therm 2015;36:25–48.
[21] P Ziółkowski, T Kowalczyk, S Kornet, J Badur On low-grade waste heat utilization from a supercritical steam power plant using an ORC-bottoming cycle coupled with two sources of heat. Energy Convers Manag 2017;146:158–173. doi:10.1016/j.enconman.2017.05.028.
[22] Z Tian, B Jiang, A Malik, Q Zheng Axial helium compressor for high-temperature gas-cooled reactor: a review. Ann Nucl Energy 2019;130:54–68. doi:10.1016/j.anucene.2019.02.032.
[23] C F McDonald Helium turbomachinery operating experience from gas turbine power plants and test facilities. Appl Therm Eng 2012;44:108–142. doi:10.1016/j.applthermaleng.2012.02.041.
[24] T Kowalczyk, P Ziółkowski, J Badur Exergy losses in the Szewalski binary vapor cycle. Entropy 2015;17:7242–7265. doi:10.3390/e17107242.
[25] D Mikielewicz, J Wajs, P Ziółkowski, J Mikielewicz Utilisation of waste heat from the power plant by use of the ORC aided with bleed steam and extra source of heat. Energy 2016;97:11–19. doi:10.1016/j.energy.2015.12.106.
[26] T W Strock, F G Russel Patent on Integral deaerator for a condenser. Elektropraktiker 1996. 0 842 688 A1.
[27] R E Athey, E Spencer Deaerating condenser boosts combined-cycle plant efficiency. Power Eng 1992;7:1–5.
[28] K Kosowski, M Banaszkiewicz, Z Domachowski, A Kosowski, M Piwowarski, R Stępień, et al. Steam and gas turbines. Principles of operation and desin. Elbląg: Alstom; 2007.
[29] Y Xu, S Hu, S Yu High temperature reactor development in China. Prog Nucl Energy 2005;47:260–270. doi:10.1016/j.pnueene.2005.05.026.
[30] A Bejan, A D Kraus Heat transfer handbook. Hoboken: Wiley; 2003.
[31] S Kakac, H Liu Heat exchangers selection, design and construction, 23; 1989. doi:10.1016/0378-3820(89)90046-5. Boca Raton.
[32] A M Y Razak Gas turbine performance modelling, analysis and optimisation. Modern gas turbine systems. Cambridge: Woodhead Publishing; 2013. p. 423–514. doi:10.1533/9780857096067.3.423.
[33] P Ziółkowski, T Kowalczyk, M Lemański, J Badur On energy, exergy, and environmental aspects of a combined gas-steam cycle for heat and power generation undergoing a process of retrofitting by steam injection. Energy Convers Manag 2019;192:374–384. doi:10.1016/j.enconman.2019.04.033.
[34] W Stanek, L Czarnowska, K Piko, M Bogacka Thermo-ecological cost of hard coal with inclusion of the whole life cycle chain. Energy 2015;92:341–348. doi:10.1016/j.energy.2015.05.042.
[35] W Stanek, J Szargut, Z Kolenda, L Czarnowska, T Bury Thermo-ecological evaluation of a nuclear power plant within the whole life cycle. Int J Therm 2015;18:121–131. doi:10.5541/ijot.72035.
[36] G Zywica, J Kicinski, T Z Kaczmarczyk, E Ihnatowicz, T Turzynski, S Bykuc Prototype of the domestic CHP ORC system : construction and experimental research. Proceedings of the 3rd International Seminar on ORC Power Systems. Brussels: University of Liège and Ghent University; 2015. p. 1–9.
[37] K Kosowski, M Piwowarski, R Stępień, W Włodarski Design and investigations of a micro-turbine flow part. Proceedings of ASME Turbo Expo 2012: Turbine Technical Conference and Exposition. Copenhagen: ASME; 2012. p. 807–814.
[38] Natalia Szewczuk-Krypa, Dorota Drosińska-Komor , Jerzy Głuch, Łukasz Breńkacz Comparison analysis of selected nuclear power plants supplied with helium from high-temperature gas-cooled reactor. Polish Maritime Research 2018;25(97):204–210. doi:10.2478/pomr-2018-0043.